Economic Geology
Vol. 78, 1983, pp. 73–90

Origin and Ore-Forming Consequences of the Advanced Argillic Alteration Process in Hypogene Environments by Magmatic Gas Contamination of Meteoric Fluids

GEORGE H BRIMHALL, JR.,

Department of Geology and Geophysics, University of California, Berkeley, Berkeley, California 94720

AND MARK S. GHIORSO

Department of Geological Sciences, University of Washington, Seattle, Washington 98105

Abstract

Possible origins for the end-stage advanced argillic wall-rock alteration assemblage have been examined and indicate a number of significant controlling factors for the generation of strongly acid hydrothermal fluids capable of hypogene oxidation and sulfidation. Metasomatic effects have been thermodynamically computed for magma-derived sulfur gases, which may contaminate convecting meteoric fluids in the monzonite K-silicate protore, and are compared with natural assemblages in the Butte district of Montana. In terms of chemical reactions, an advanced argillic assemblage results from a leaching interval characterized by a barren quartz-pyrite-muscovite assemblage in which no clay minerals are stable at 300°C, a temperature characteristic Main Stage fluid circulation. High oxygen and sulfur fugacities characteristic of the advance argillic assemblage, following this so-called S-type assemblage of intermediate age between the Main Stage (veins) and pre-Main Stage hydrothermal (protore) events, are critical to the initiation and continuation of major base metal remobilization processes affecting the protore and the ultimate formation of Main Stage high-grade veins.

The advanced argillic assemblage with covellite is produced in hypogene environments at 300°C by sulfur metasomatism of protore only for a limited range of net sulfur valences, essentially −1 to +2, placing limiting constraints on the possible ratios of SO_2 and H_2S gases. A second important factor in the formation of the advanced argillic assemblage is the relative reaction rates of protore and contaminating sulfur gases. If the gases react at a rate which is too low, wall-rock feldspars remain continuously stable, buffering solution pH at too high a value to produce a strong hydrolytic attack of the protore or to affect copper remobilization by oxidation. Contamination by sulfur gases is a third factor of importance since continued reaction beyond the advanced argillic assemblage results in pH increase, sulfide deposition, and final attainment of feldspar stability. A final factor of major importance reveals the reason for the pivotal role of this assemblage to the geochemical evolution of ore-forming systems. It is that a minimum negative net volume of reaction causes, by wall-rock dissolution and fracture enlargement, the high permeability necessary for circulation of enormous quantities of hydrothermal fluids and vein growth characteristic of this extreme alteration facies.

Introduction

MAIN STAGE copper vein formation at Butte, Montana, has been shown, at least in part, to be due to hydrothermal scavanging, transport, and reprecipitation of copper originally deposited five million years earlier in an immense, fracture-controlled, disseminated sulfide potassium-silicate protore which represents the primary distribution of hypogene copper-iron sulfide mineralization (Brimhall, 1977, 1979, 1980). The hydrothermal copper remobilization process, occurring at much lower temperatures (300°C) than the porphyry copper-type protore formation (600°C), appears to be a late-stage hypogene oxidation effect resulting from deep circulation of heated meteoric water driven by a relatively young intrusive complex in the central part of the district where the most intense alteration occurs.

In this paper we are reporting on a preliminary investigation of the possible origins of one other ore-forming element in the late Main Stage mineralization, i.e., sulfur, which shows a distribution pattern related not to the early protore but to the late-stage porphyry intrusives in the Central zone in which the high sulfur fugacity pyrite-covellite-digenite-(chalcocite) mineralization in horsetail structures is often part of the advanced argillic alteration assemblage. Therefore, sulfur, in contrast to copper, may have been added metasomatically to the hydrothermal system, possibly through magmatic gas contamination of circulating meteoric water, with the major flux being in the Central zone. Most important has been

0361-0128/83/119/73-18$2.50

to determine whether or not the advanced argillic alteration assemblage was generated by progressive sulfidation and oxidation of fluids migrating upward through the monzonite-potassium-silicate protore. If so, then a complete reaction cycle for the formation of deeply circulating acid hydrothermal fluids may be envisioned for the Butte district. It would encompass near-surface precious and base metal mineralization, intermediate-level polymetallic base metal vein systems, and an older, deep-level protore mass cut by late veins containing essentially the same sulfides as the protore, i.e., pyrite, chalcopyrite, and bornite. The ultimate origin of all the metals and nonmetals in the complete system may, in actuality, be complex and quite varied from element to element, e.g., copper from the protore; sulfur, arsenic, chlorine, and perhaps other volatiles from the late magmatic system; iron from sericitization of wall-rock mafic minerals; and perhaps other elements from near-surface meteoric water convection and oxidation. However, we do not mean to suggest that copper in the protore formed by the same processes as those associated with the later veins.

This paper focuses on the origin of one late phenomenon, i.e., the advanced argillic assemblage, in an effort to understand better the pivotal role it plays in the systematic evolution of deeply circulating acid ore-forming fluids within the Butte district as well as in base and precious metal deposits in general. It has been shown that this advanced argillic alteration assemblage with pyrite and covellite represents an end stage of Butte vein-forming processes, including extreme acidity, base leaching capability, state of oxidation and sulfidation, and level of textural destruction of the wall rock (Brimhall, 1980). All other vein assemblages studied within the protore mass appear to represent various intermediate states of reaction of quartz monzonite wall-rock protore with late acid hydrothermal fluids capable of ultimately generating the advanced argillic alteration assemblage (kaolinite-muscovite-alunite-quartz). For example, deep-level pyrite-chalcopyrite (bornite) veins may represent copper remobilization within a hydrothermal system chemically buffered by the subsurface pyrite-chalcopyrite-magnetite K-silicate protore. Upper level chalcocite-bornite veins formed above the dome-shaped protore mass, apparently escaping its full chemical buffering influence. Central zone horsetail pyrite-covellite-(chalcocite) assemblages occur within a pervasively sericitized wall rock in which all early buffer mineral assemblages have been destroyed, allowing the system to evolve to a fluid-dominated state, in marked contrast to the wall rock-dominated vein systems. It is in this Central zone environment that the most O^{18}-depleted fluids occurred (Sheppard and Taylor, 1974) and are thought to represent the most pristine ore-forming fluids.

The mass transport medium responsible for vein formation appears to be part of a very large chemical system which was essentially closed during the Main Stage hydrothermal event with respect to copper. More simply, there is as yet no concrete geologic evidence in available exposures which suggests that the late-stage magmatic activity actually introduced economically important quantities of copper. Instead, the copper was essentially remobilized from a low-grade protore state to a more concentrated one; this leached and highly oxidized and sulfidized protore relict forms a necessary complement of the high-grade vein formation within the district. We are therefore interested in gaining insight into the processes by which such barren pyrite-quartz-sericite assemblages form, so that a proper interpretation of their occurrence within a district zonation pattern may be made for other deposits. As deep mineral exploration continues, improved understanding of the complete zoning pattern, including well-mineralized as well as barren phases, becomes essential. It is obvious that a knowledge of the immediate source of ore-forming elements, both metals and nonmetals, would help considerably in defining deep exploration targets elsewhere.

Previous Work

The origin of wall-rock alteration mineral assemblages and related intensely acid hydrothermal fluids has been greatly elucidated by recent experimental studies (Hemley and Jones, 1964; Hemley et al., 1969, 1980) as well as by stable isotope investigations of ore deposits (Taylor, 1974; Sheppard and Taylor, 1974). From these efforts it is apparent that ore-forming fluids capable of producing strong hydrolytic attack of wall rocks at temperatures around 300°C are largely meteoric in origin in terms of the water component, and contain a large proportion of ionized constituents with a low cation/H^+ activity ratio (Hemley and Jones, 1964). It is thought that such fluids may be generated by the influx of juvenile gases into heated meteoric water and by the oxidation of pyrite and magmatic H_2S (Hemley and Jones, 1964; White, 1957). Hemley, in particular, has favored this origin for the advanced argillic alteration assemblage at Butte by the "continued accession of acid volatiles as the system cooled in Main Stage meteoric time, incorporating a certain amount of entrained ionizing halogen acids as well as sulfur acids" (J. J. Hemley, pers. commun.). Recent solubility experiments have shown how magmatic aqueous phases might be generated through strong partitioning away from the silicate melt phase of chlorine, sulfur, carbon dioxide,

and heavy metal chloride complexes (Burnham and Ohmoto, 1980). These studies point out that because of the high concentration of SO_2 relative to H_2S in magmatic aqueous phases, increasing f_{O_2} and decreasing pressure may produce a highly sulfur-rich fluid capable of transporting significant amounts of heavy metal chloride complexes. Two distinct felsic magma types, i.e., I-type and S-type (Chappell and White, 1974) may have very different SO_2/H_2S fugacity ratios and may ultimately give rise to porphyry copper deposits (0.1 to 10, high f_{O_2}) or porphyry tin deposits (much less than 0.01, low f_{O_2}) (Burnham and Ohmoto, 1980). These arguments have been used to explain high-temperature, late-magmatic ore-forming processes, including hydrofracturing mechanisms, but the lower temperature vein systems such as those at Butte probably require a fundamentally different set of concentration mechanisms involving dominantly meteoric water. The origin of the sulfur in the Main Stage fluids, and particularly the processes by which it was incorporated into circulating meteoric fluids, is a major concern of this investigation.

This problem is more complicated than is generally presented in the published literature. Although it is often true, as pointed out by Burnham and Ohmoto (1980), that meteoric water may serve only to modify features formed earlier by magmatic processes involving dominantly magmatic water, nevertheless the formation of immense late-stage vein systems involves remobilization and multicomponent metasomatism on an enormous scale, extending well beyond the limits of the protore mineralization, both vertically and laterally. It is in this extreme case that the relative importance of complex meteoric phenomena is seen in relation to relatively simple deep subsurface low-grade protore formation (Brimhall, 1977, 1979). There is still very little understanding of the complex transitional processes, of both a chemical and a physical nature, by which magmatic-hydrothermal systems may evolve upward into lower temperature overlying vein networks dominated by meteoric fluids. It is also apparent that the late-stage vertical and lateral remobilization of ore-forming elements can produce exploration targets considerably larger than the original dimensions of the protore. The redistributive phenomena described is much more than simple modification of magmatic and postmagmatic mineralization. The special geological circumstances and requisite metasomatic behavior necessary to cause major redistributive effects have not been previously described in the literature, except for secondary enrichment processes occurring during supergene oxidation.

We hope in this paper to describe possible mechanisms by which meteoric fluids may become quite reactive with respect to surrounding protore mineralization through mixing with late-stage magmatic gases emanating from the Central zone. The composition of such gases is uncertain, but it is worth noting that between the years 1880 and 1964, over 300 million pounds of arsenic compounds were produced from the Butte district in addition to great quantities of sulfuric acid. Furthermore, numerous other deposits contain major amounts of enargite or tennantite, e.g., Tintic and Magma in the United States and especially many large porphyry-related deposits—Chuquicamata, El Salvador, Potrerillos, and El Teniente as well (Hollister, 1978; Peterson, 1980)—in South America. It is possible, therefore, that late-stage modification processes in extremely large ore-forming systems may quite often involve the major introduction of some critical elements, e.g., sulfur and arsenic, and the redistribution of others. The chemical origin of the advanced argillic assemblage presented was discussed qualitatively by Meyer and Hemley (1967) but is quantitatively assessed in the present paper; in addition the importance of the process to the remobilization and reconstruction of the entire Butte system at the higher levels in Main Stage time is pointed out and demonstrated.

Method

The likely consequences of sulfur gas contamination of meteoric water and the subsequent reaction of this aqueous fluid with protore minerals may be estimated by simulating irreversible chemical reactions using the approach of Helgeson (1968, 1971), computer programs (EQ3-EQ6) of Wolery (1979), and the thermodynamic data base of Helgeson et al. (1978) and Wolery (1979). The compositional characteristics of an aqueous phase progressively equilibrating with product mineral species while reactant minerals and gases are continually added to the closed chemical system have been computed as a function of the overall chemical reaction progress. A temperature of 300°C and a pressure of 500 kb were chosen as representative of conditions under which Main Stage processes have occurred (Meyer et al., 1968; Brimhall, 1979, 1980). The sequence of events produced by the simplified isothermal-isobaric thermodynamic calculations applies to a specific place within the protore through which the vein-forming fluid flows, and to the sequential changes in fluid composition and associated mineral assemblage. Dissolution of K-silicate protore minerals takes place at a rate determined lithologically (Brimhall, 1979) and used in a previous study (Brimhall, 1980) in which the protore mineral abundance, i.e., number of moles as well as relative reaction rates, is given normalized

TABLE 1. Equivalence Table of Computational Gas Species

Average sulfur valence	Likely natural gas species	Computational species
[+4]	$SO_{2(g)}$	$1/2\ S_{2(g)} + O_{2(g)}$
[+3]	$5/6\ SO_{2(g)} + 1/6\ H_2S_{(g)}$	$1/2\ S_{2(g)} + 3/4\ O_{2(g)} + 1/6\ H_2O_{(l)}$
[+2]	$2/3\ SO_{2(g)} + 1/3\ H_2S_{(g)}$	$1/2\ S_{2(g)} + 1/2\ O_{2(g)} + 1/3\ H_2O_{(l)}$
[+1]	$1/2\ SO_{2(g)} + 1/2\ H_2S_{(g)}$	$1/2\ S_{2(g)} + 1/4\ O_{2(g)} + 1/2\ H_2O_{(l)}$
[0]	$1/3\ SO_{2(g)} + 2/3\ H_2S_{(g)}$	$1/2\ S_{2(g)} + 2/3\ H_2O_{(l)}$
[−1]	$1/6\ SO_{2(g)} + 5/6\ H_2S_{(g)}$	$1/2\ S_{2(g)} + 1/3\ H_2O_{(l)} + 2/3\ H_{2(g)}$
[−2]	$H_2S_{(g)}$	$1/2\ S_{2(g)} + H_{2(g)}$

The table represents a net valence spectrum of natural gas species likely to be derived from silicic magmas from pure SO_2 (+4 sulfur valence, i.e., most oxidized) to pure H_2S (−2 sulfur valence, i.e., most reduced)

to 1.0 mole of protore chalcopyrite as follows: annite (biotite) (3.49), magnetite (1.97), K-feldspar (8.89), pyrite (0.548), quartz (44.45), and low albite (plagioclase) (16.22). The sum of these stoichiometric reaction coefficients (v) is 81.5 moles and remains constant throughout the calculations (see Table 1).

Starting fluid composition

The aqueous fluid with which these protore minerals reacted is in chemical equilibrium with respect to the protore minerals and has the following properties: pH = 5.6, $\log f_{O_2} = -33.0$, $\log f_{S_2} = -10.77$, $\log H_2S_{(g)} = -0.99$, $\log f_{H_2O_{(g)}} = 1.91$, $a_{H_2O_{(liq)}} = 0.98$; with the following molal concentrations: Na (0.6378), K (0.0658), Al (0.0012), Si (0.0122), Cl (0.7025), S (0.0029), Fe (0.00001), and Cu (0.00022). The abundance of elements which are not fixed by mineral solution equilibrium, i.e., sodium and chlorine, is consistent with previous mass transfer calculations (Brimhall, 1980) on copper remobilization at Butte. Physically, we are concerned with a point within the fresh protore in which a Main Stage fracture develops and along which hydrothermal fluid migrates upward. At the start of the reaction the fluid is locally in equilibrium with all the protore minerals.

Reaction constituents

Into the fluid which is in equilibrium with the protore we have introduced various amounts of protore, sulfur gases, and $H_2O_{(l)}$ in an effort to discover the importance of sulfur gas contamination and groundwater dilution effects relative to reaction rates of protore minerals. Burnham and Ohmoto (1980) have pointed out that the most likely species accounting for the transport of sulfur in supercritical fluids emanating from silicic magmas are H_2S and SO_2. Their experimental observations are consistent with values of intensive variables from phenocryst assemblages found in siliceous lavas. An examination of Fe-Ti oxide equilibria in rhyolites (I. S. E. Carmichael and M. S. Ghiorso, in prep.) provides values for liquidus temperatures and oxygen fugacities that suggest an equilibrium distribution of gaseous sulfur species ranging from pure H_2S to $H_2S \cdot SO_2$ mixtures to pure SO_2 depending on the composition and water content of the magma. Equilibrium calculations rule out the predominance of other sulfur gases (i.e., S_2, SO_3, etc.) under P, T, and f_{O_2} conditions likely to be found in the crust. Clearly, contamination of the protore fluid assemblage by ascending magmatic gas streaming from a young siliceous intrusive complex must involve the metasomatic introduction of sulfur whose SO_2/H_2S (or oxidation state) ratio might be quite variable. If the escaping emanations equilibrate thermally with their surroundings while en route to their joining with the protore (at 300°C), and do so while remaining chemically inert, thermodynamic calculations demonstrate that all the sulfur will be transformed to SO_2. On the other hand, if thermal equilibration is accompanied by protore buffering of the fugacity of oxygen, then the dominant sulfur species will be H_2S. Partial equilibration, whether thermal or chemical, will of course yield intermediate effects. We have chosen, in this paper, to examine sulfur gas contamination of the protore by the whole spectrum of natural magmatic mixtures of H_2S and SO_2, with the hope of placing H_2S/SO_2 ratio limits on likely Main Stage ore-forming solutions. The addition of H_2S and SO_2 in varying amounts can be modeled as the introduction of equivalent masses of sulfur, hydrogen, and oxygen. This is possible because we are simulating an irreversible chemical process where the reactants, within the interval modeled (see below), do not achieve chemical equilibrium with the fluid phase and alteration products. Given this fact, we have considered it convenient to model the introduction of magmatic SO_2 and H_2S into the protore-equilibrated fluid by using the gaseous species H_2, S_2, O_2, and H_2O, not SO_2 or H_2S. Table 1 is provided to demonstrate that

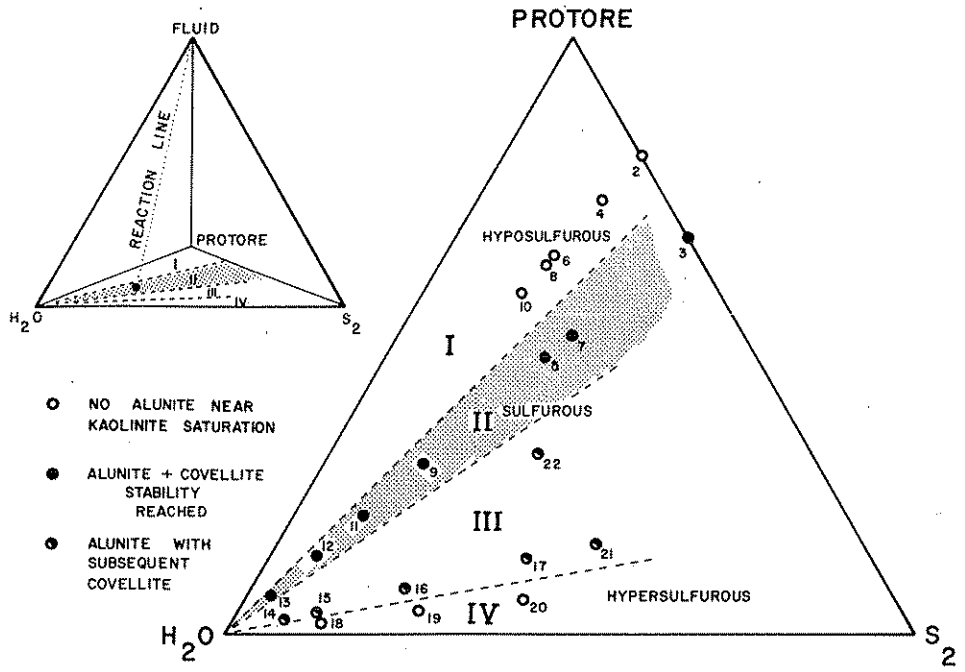

FIG. 1. Stoichiometric reaction coefficient (reaction rate) diagrams showing the relative position of each model calculation (run) which is represented (Fig. 1, left) by a reaction line extending from the base of the tetrahedron (fluid-H_2O-S_2-protore) to the fluid apex. The calculation proceeds from the base to the upper fluid apex as reactant material is titrated into 1,000 grams of fluid. The reaction rates of the constituents, i.e., H_2O, S_2, and protore, are specified and are constant for each run. The fluid composition, too, is specified at the start of the run to be in equilibrium with the quartz monzonite protore and to contain chloride as discussed in the text. Thermodynamic results for the various calculations are shown in the right-hand figure and may be grouped in four distinct zones (I-IV), each characterized by a similar predicted mineral assemblage and pH (acidity) behavior.

just as the natural sulfur species SO_2 and H_2S can be combined in varying proportions to span the sulfur valence spectrum of +IV to −II, so can our species (H_2, O_2, H_2O, and S_2). We have elected to direct our attention initially toward the chemical effects of a metasomatic introduction of neutral valent sulfur and to explore the coincident contamination of the protore gas mixture with H_2O, i.e., to simulate dilution with shallow meteoric and/or juvenile water. Subsequent to our discussion of the effects of dilution we will explore the consequences of the addition of sulfur gases spanning the whole valence spectrum (Table 1).

The reaction coefficients, i.e., reaction rates of each of the 22 preliminary zero sulfur valence calculations using $S_{2(g)}$, protore, and $H_2O_{(l)}$, are shown in Figure 1. The tetrahedron shown represents the starting fluid at the top into which a fixed proportion of each of the three reactants for each calculation are introduced, i.e., H_2O, protore, and $S_{2(g)}$, shown by their position on the base of the tetrahedron. Reaction proceeds along a reaction line as shown in Figure 1 for a single path calculation. The base of the tetrahedron (Fig. 1, enlarged on the right) shows the reaction coefficients, or rate constants, of each of the reactants for each of the 22 runs. The numerical values for the rate constants used in each calculation are also given in Table 2. Notice that the total protore rate constants, i.e., the sum of the individual rate constants of each protore mineral, is always 81.5 (see note in Table 2) in contrast to those of H_2O and S_2 which vary over the triangular area in Figure 1. For example, consider in Figure 1, run (2) in which 81.5 moles of protore (composed of 1.0 moles of chalcopyrite, 3.49 moles of biotite, 1.97 moles of magnetite, 8.89 moles of K-feldspar, 5.48 moles of pyrite, 44.45 moles of quartz, and 16.22 moles of albite) react with 20.375 moles of $S_{2(g)}$.

Results Using $S_{2(g)}$

Reaction characteristics have been computed for the 22 compositions given in Figure 1 and Table 2 using protore, $H_2O_{(l)}$, and $S_{2(g)}$ as reactants with chloride-bearing neutralized fluid. The results may be effectively described in terms of the similarity of the thermodynamically predicted mineral assemblages to those found in nature characterized by the advance

TABLE 2. Stoichiometric Reaction Coefficients Used in Model Calculations for Neutral Valence Sulfur Species

Run no.	Region in figure 1	Stoichiometric reaction coefficients		
		ν_{H_2O}	$\nu_{Protore}$ [1]	ν_{S_2}
2	I	0	81.5	20.375
3	II	0	81.5	40.75
4	I	10.1875	81.5	20.375
5	II	54.33	81.5	40.75
6	I	27.167	81.5	20.375
7	II	40.75	81.5	40.75
8	I	30.5625	81.5	20.375
9	II	163.0	81.5	40.75
10	II	40.75	81.5	20.375
11	II	285.25	81.5	40.75
12	II	489.01	81.5	40.75
13	II	1,100.26	81.5	40.75
14	III	2,934.0	81.5	244.5
15	III	1,874.31	81.5	244.5
16	III	760.67	81.5	244.5
17	III	326.0	81.5	244.5
18	IV	3,694.67	81.5	570.5
19	IV	1,521.3	81.5	570.5
20	IV	765.39	81.5	570.5
21	III	211.9	81.5	249.92
22	III	108.67	81.5	81.5

[1] Protore is composed of the following minerals with reaction coefficients as given: chalcopyrite (1.0), annite (biotite) (3.49), magnetite (1.97), K-feldspar (8.89), pyrite (5.48), quartz (44.45), and low albite (plagioclase) (16.22), summing to 81.5

argillic assemblage at Butte. The standard of comparison is, therefore, an alteration mineral assemblage consisting of quartz, kaolinite or pyrophyllite, muscovite (sericite), alunite, pyrite, and covellite. During the course of the irreversible reactions, one or more of these necessary phases may be thermodynamically stable, but for the reaction to have significance as far as the actual generation of the advanced argillic assemblage, all the phases should be stable simultaneously at some point in the reaction progress (ξ).

The results of such reaction path calculations are shown in Figure 1, in which there are four well-defined zones, i.e., I, II, III, and IV, each typified by a different degree of similarity to the advanced argillic assemblage. The reaction coefficients for each run (1–22) are represented by various symbols, depending on the stability, at some point during the reaction of minerals of critical importance to the advanced argillic assemblage: no alunite (zone I and IV), simultaneous stability of alunite and covellite (zone II), and alunite with subsequent covellite (zone III). In all cases saturation of these phases in addition to muscovite, quartz, and pyrite occurred. Kaolinite, a mineral most characteristic of the advanced argillic assemblage, did not reach true saturation (affinity = 0.0), but in zones II, III, and IV, its affinity at some point in the reaction progress was well within experimental error of its standard heat of formation (M. S. Ghiorso, pers. commun.) and was therefore very probably within the limits of saturation. This behavior is probably the result of small uncertainties in the standard thermodynamic data of the kaolinite used. In addition we have modeled the system as being calcium free.

In this regard, Main Stage alteration takes place by conversion of Butte quartz monzonite andesine plagioclase to montmorillonite, followed by replacement of this phase by kaolinite, and in turn by sericite, with a loss of calcium to the vein fluid. However, we have modeled the reaction using a calcium-free simplification, resulting in the direct replacement of plagioclase (albite) by muscovite, a process which is based on textural evidence of the so-called S type assemblage (Meyer et al., 1968). This alteration assemblage involves quartz-pyrite veins with sericitic alteration envelopes without the concentric clay envelopes characteristic of typical Main Stage assemblages. It is likely that the S assemblage is intermediate in age between the pre-Main Stage K-silicate protore event

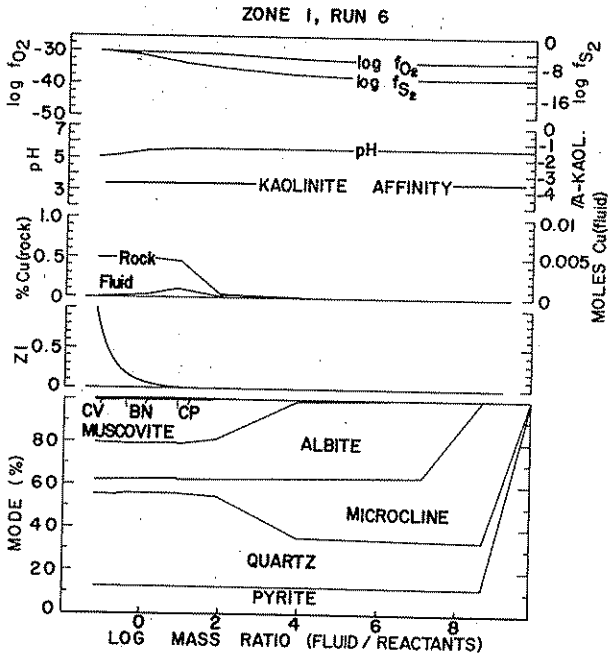

FIG. 2. Reactions produced in zone I (Fig. 1) as a function of fluid/reactant mass ratio (abscissa). Predicted modal variation is shown in volume percent near the bottom of the figure. Reaction, as calculated, proceeds from right to left in the figure. Notice that protore feldspars are stable over the entire span of reaction, although muscovite is stabilized late in the reaction history. Notice montonous high pH and low kaolinite affinity curves. Very little copper is contained in the aqueous fluid phase in this type of reaction. Most of the reaction variation occurs at low values of the reaction progress variable (ξ).

and the Main Stage (Meyer et al., 1968). We therefore feel that kaolinite saturation occurred only with the advanced argillic assemblage; this is consistent with geological reality and the calculation scheme used is not an oversimplication of the processes involved.

The zones characterizing the attainment of conditions representative of the advanced argillic assemblage (Fig. 1) are apparently bounded by lines emanating from the reactant $H_2O_{(l)}$. The dominant controlling factors in the formation of the advanced argillic assemblage, therefore, apparently relate only to the relative reaction rate ratio of protore to $S_{2(g)}$, not to the relative amount of H_2O. Dilution effects resulting from an input of $H_2O_{(l)}$ are likely to be only on a second order of importance at most. This is because the advanced argillic assemblage, when reached, occurs at low values of the reaction progress variable before the relative addition of H_2O becomes important.

The calculated sequence of modal variations and the solution composition evolution for runs typical of each of the four zones (I–IV) are given in Figures 2 (zone I, run 6), 3 (zone II, run 5), 4 (zone III, run 17), and 5 (zone IV, run 20). The abscissa in Figures 2 to 5 is proportional to the reaction progress (ξ) as shown

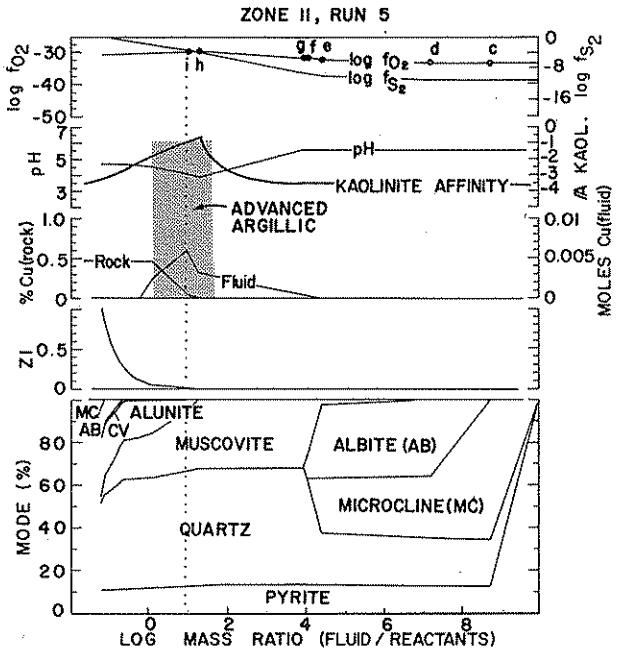

FIG. 3. Reactions in zone II (Fig. 1) as a function of fluid/reactant mass ratio. Notice, as the reaction proceeds from right to left, the destruction of wall-rock protore feldspars as quartz and muscovite grow accompanied by pyrite. The advanced argillic alteration mineral assemblage is reached in the stippled region at a minimum in solution pH and at maximas in kaolinite affinity (in k-cals), oxygen fugacity, and copper content of the coexisting aqueous fluid. Feldspars restabilize as the reaction continues.

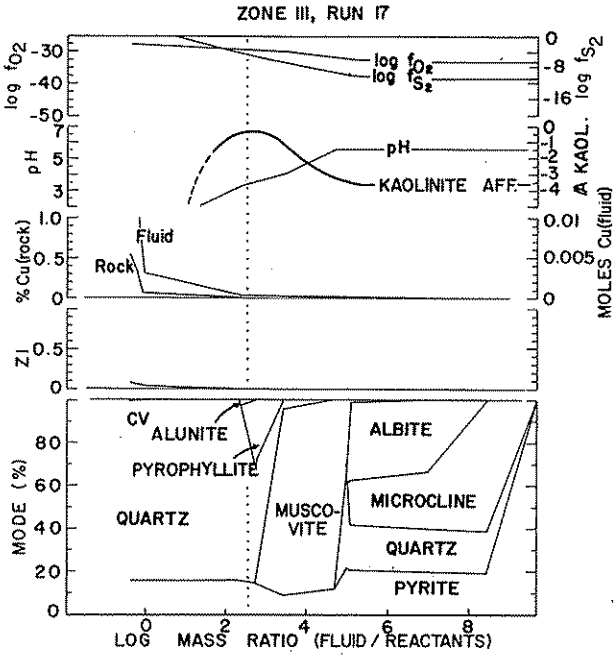

FIG. 4. Reactions in zone III (Fig. 1). They are grossly similar to the advanced argillic region shown in zone II (Fig. 3). This zone produces covellite growth following alunite and pyrophyllite stabilization. Notice maxima in the pH curve. This reaction sequence differs mainly in the low solubility of copper during kaolinite stability. Zone III may be more typical of barren advanced argillic assemblages than those in base metal-rich hydrothermal systems.

but increases from right to left. The reactions were computed from right to left in the figures and are represented here as the log mass ratio (fluid/reactants) using a 1,000-g starting fluid reservoir. The results will be discussed, zone by zone, starting with zone I.

Zone I

In this region in which very little neutral valence sulfur gas (Table 1) reacted with protore and $H_2O_{(l)}$, the results shown in Figure 2 imply continuous feldspar stability with no production of alunite. The nearly flat pH profile reflects this feldspar stability, remaining at a value above 5.0. The reactions in zone I are not at all indicative, at any point, of advanced argillic assemblages.

Zone II

In zone II, a higher neutral valence sulfur gas/protore reaction rate ratio produces effects which are very similar to natural advanced argillic assemblages and to known sequences of mineral assemblages as well. An interruption in feldspar saturation is of paramount importance in this regard. As is known, feldspar stability is one of the most useful field criteria for characterizing alteration types. It is significant,

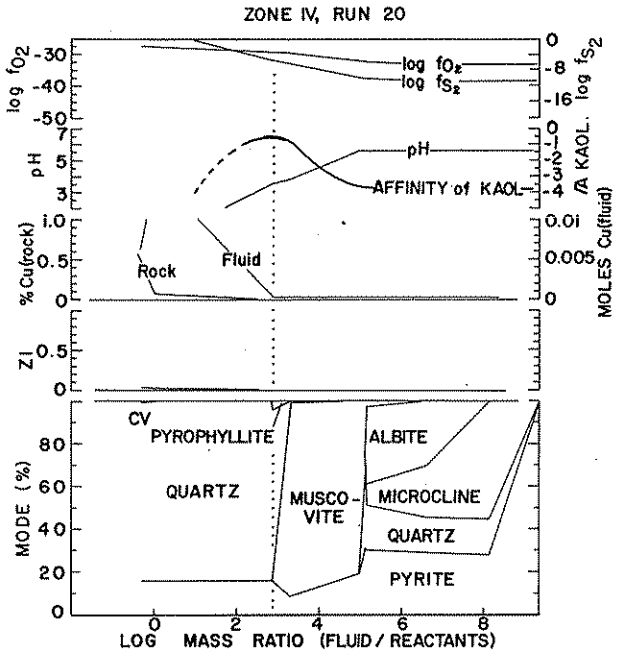

FIG. 5. Reaction sequence in hypersulfurous zone IV is shown including rapid pH decrease, right to left, as well as the lack of alunite.

therefore, that as the reaction proceeds from right to left, feldspars are initially stable. While protore, neutral valence sulfur and $H_2O_{(l)}$ continue to react, however, both feldspars are precipitated as a copper-barren quartz-muscovite-pyrite assemblage which becomes stable over a very protracted interval of fluid/rock ratio, but not necessarily over a long period of geologic time.

It is very significant that as the reaction continues to the left beyond this barren quartz-pyrite-muscovite assemblage, covellite reaches saturation simultaneously with alunite, at a fluid/rock ratio value (or ξ) at which kaolinite is within experimental error of saturation. This assemblage and interval of reaction progress is shown in gray in Figure 3 and represents the advanced argillic assemblage exactly. The composition of the fluid phase, too, is worth noting. The solution pH goes through a minimum value at this mineral assemblage, precisely at the point of near-kaolinite saturation. The log f_{O_2} is a maximum value near −30, while log f_{S_2} is continuously increasing. Obviously, as the reaction continues it proceeds past the advanced argillic assemblage as protore mineral buffers take over and feldspar saturation is again attained, causing the ultimate increase in solution pH.

Zone III

In contrast to zone II, reactions in this zone produce solution pH values which ultimately reach exceedingly low—probably unrealistic—levels: well below 3.0. It is worth noting, nevertheless, that at intermediate fluid/rock ratio values (ξ), the assemblage pyrite-quartz-muscovite-pyrophyllite-alunite is thermodynamically stable, although covellite is not saturated until later.

Zone IV

In this region no alunite is produced, nor is there a maximum produced in log f_{O_2} as in zone II. Zones III and IV both have this maximum, implying that as neutral valence sulfur continues to react, oxidation effects proceed uninterrupted by the buffering action of the protore, in contrast to zone II.

Solution composition variation

Figures 6 to 8 present computed phase diagrams and reaction paths for each of the four zones (I–IV) using the same runs typical of each zone as used in figures 2 to 5. In each of Figures 6 to 8 the reaction starting point is shown as a hexagon. We see in Figure 6 a standard sulfur-oxygen fugacity diagram in which the various reaction paths are shown covering quite similar trajectories. The main feature of significance for zone II is that, as the reaction path goes through

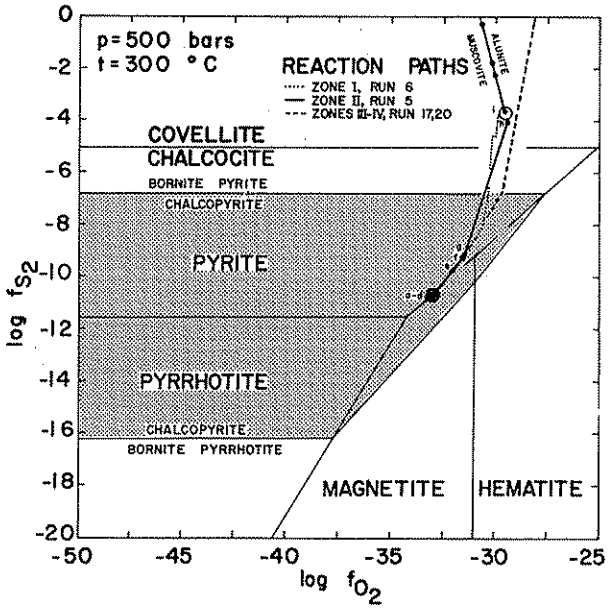

FIG. 6. Sulfur-oxygen fugacity diagram showing the stability fields of oxides and sulfides including protore chalcopyrite (stippled) and reaction paths for each of the zones I to IV extending from the magnetite-chalcopyrite protore (hexagon at point a). Only reactions in zone II (solid heavy line) extend from the protore (hexagon point (a)) and ultimately turn along the alunite-muscovite phase boundary. Zone II reaction path intersects this phase boundary approximately at the covellite-chalcocite phase boundary, reflecting quite well the high sulfur fugacity assemblage found in nature.

a maxima in log f_{O_2} (changing slope from positive to negative), muscovite-alunite equilibria is attained (Brimhall, 1980). Reference points are shown as letters (a to i) in both Figures 6 to 8 and 3. Point i, reached in zone II, represents quite adequately the advanced argillic assemblage. Reaction paths through stability fields of alteration silicates are shown in Figure 7. Notice especially the traverses through the muscovite field (at quartz saturation) in zones II, III, and IV. Ideally, the Butte advanced argillic assemblage occurs at the triple point muscovite-kaolinite-alunite. It is apparent that the main difference between the zone II path and those of zones III and IV is that high levels of reaction in zone II produced an alunite-muscovite equilibrium, deflecting the path upward toward higher values of log $(a^2_{K^+}\, a_{SO_4^{-2}})$, or put differently, that the acidity was sufficiently low so that muscovite was able to buffer the system along the alunite boundary.

In Figure 8, a marked departure in reaction paths is seen between paths for zones I and II and zones III and IV. As reactions proceed from the initial protore composition (hexagon), the paths diverge at point g where the runs of zones III and IV change slope abruptly and go toward higher values of log $(a_{Fe^{+2}}/a^2_{Cu^+})$. This occurs because of an apparent sudden increase in pyrite solubility resulting in a modal decrease of pyrite at a log mass ratio (fluid/

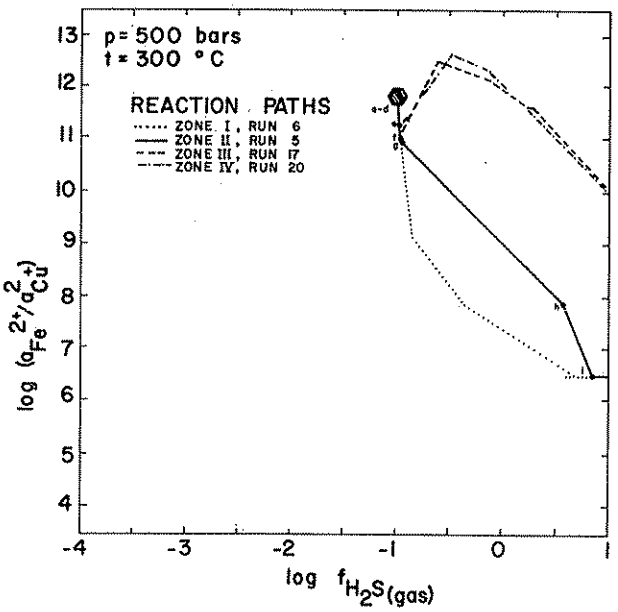

FIG. 8. Activity-fugacity diagram showing reaction paths typical of each of the zones I to IV emanating from the protore assemblage (hexagon). Notice the divergence of paths for zones I and II and paths of zones III and IV near points e to g. This increase in Fe/Cu^+ activity ratio is due to pyrite dissolution occurring only in zones III and IV (see Figs. 4 and 5). In contrast, pyrite in zones I and II (Figs. 2 and 3) does not undergo reduction in modal values.

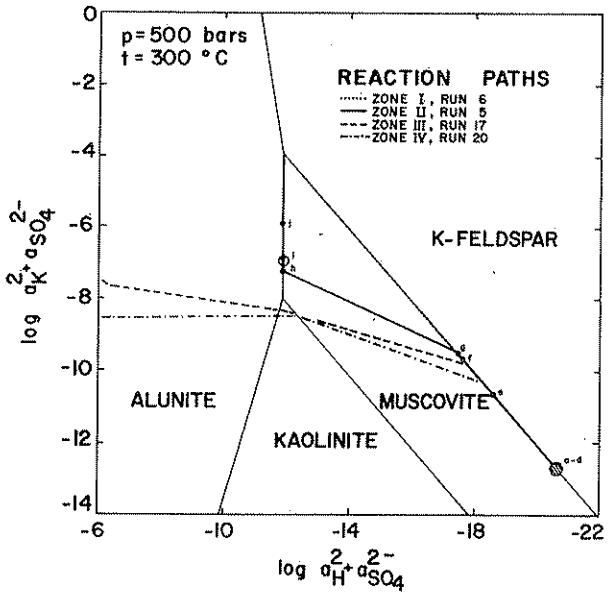

FIG. 7. Activity diagram at quartz saturation showing stability fields of alteration minerals and reaction paths for zones I to IV events. Advanced argillic assemblage is best represented by the triple point kaolinite-alunite-muscovite in the presence of quartz. Reactions all proceed from the protore assemblage at a to d (hexagon).

reactants) of 5 in Figures 4 and 5 but not in Figures 2 and 3. In Figure 8, the advanced argillic assemblage is reached only along the path for zone II at point i. The phases present which buffer the activity products log $(a_{Fe^{+2}}/a_{Cu^+})$ will be discussed more fully in a later section.

Discussion of Neutral Valence Metasomatism in Zones I to IV

On the basis of the analysis presented, it is clear that zone II computed reaction products best match the advanced argillic high sulfur ore assemblage in nature as simultaneous covellite-alunite-kaolinite-muscovite saturation is concerned. Zone I can be thought of as having a neutral valence sulfur supply too low relative to protore reaction rates to result in feldspar destruction and reprecipitation of potassium as alunite. It is therefore hyposulfurous (Fig. 1). Zone II reactions have exactly the proper proportion of neutral valence sulfur protore to produce the desired assemblage. It is referred to here as sulfurous. Zone III produces the advanced argillic assemblage but with covellite only at late stages. Zone IV is hypersulfurous because too much sulfur is added to produce the full complement of Butte advanced argillic assemblage minerals including alunite.

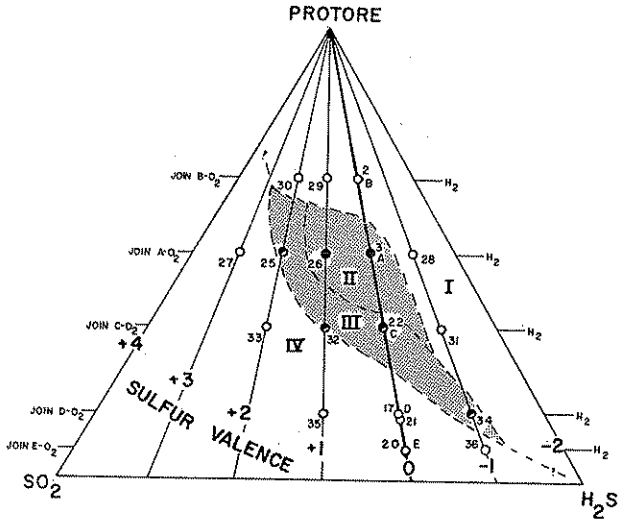

FIG. 9. Reaction rate values for calculations covering the full valence spectrum of sulfur-bearing gases, i.e., SO_2 (+4) to H_2S(−2). Individual reaction runs are indicated by a small circle and index number (see Tables 2 and 3). Isovalence lines emanate from the protore corner. Reaction zones I to IV are shown. Zone I is parallel to the protore-H_2S side at very low values of SO_2, i.e., oxidized sulfur. Zones II and III also lengthen parallel to the protore-H_2S side and occur at intermediate values of SO_2. Zone IV occurs at relative high values of SO_2. The advanced argillic alteration assemblage has a limited sulfur valence range, i.e., −1 to about +2.

Results Using the Valence Spectrum of Sulfur

The calculations presented for zones I to IV so far provide preliminary information on the possible manner in which the advanced argillic alteration assemblage is formed under hypogene conditions in the Butte district, assuming of course that neutral valence sulfur is the main sulfur species acting as a contaminant of circulating ground water. However, it is imperative to consider the nature and valence spectrum of more likely magmatic gases. In Table 1 we have presented a spectrum of such sulfur gases, both in terms of natural mixtures of $SO_{2(g)}$ and $H_2S_{(g)}$ as well as their present computational equivalents using $S_{2(g)}$, $O_{2(g)}$, $H_{2(g)}$, and $H_2O_{(l)}$. We show in Figure 9 the triangular reaction coefficient diagram for the most likely natural magmatic gases, emphasizing the relative position of isovalence sulfur gas species: [+4], [+3], [+2], [+1], 0, [−1], and [−2]. Notice in Figure 9 that the position of the neutral valence ($S_{2(g)}$) reactions (1–22) is given by a heavy line. Because the desired advanced argillic assemblage is attained only in zones II and III, it is necessary to investigate the extensions of these zones into geologic environments characterized by both higher and lower valence sulfur gas contamination. This has been undertaken by computing nine more exploratory path runs, labeled 25 to 36, in Figure 9. The relative reaction rate coefficients lists in Table 3 (Fig. 9) may be derived from the equivalence of likely and computational species given in Table 1 for each sulfur valence state. These relationships are depicted graphically in Figure 10A and B for $O_{2(g)}$ and $H_{2(g)}$ reactions along the linear joins as shown (A, B, C, D, and E).

The geometric relationship of the natural and computational sulfur gas species may be easily visualized as shown in Figure 11 which includes, in addition to $O_{2(g)}$, $S_{2(g)}$, and $H_{2(g)}$, both protore and $H_2O_{(l)}$. The region in which the advanced argillic assemblage is predicted is shown in relation to isovalence sulfur lines.

Importance of the Advanced Argillic Assemblage to Mineralization Processes

Spatially and temporally the advanced argillic assemblage occurs at a critical position in the Butte district, offering key information for the interpretation of the alteration, mineralization, structural zonation, and chemical evolution of the Main Stage hydrothermal event. The occurrence of the high sulfur assemblage within the Central zone accompanied by advanced argillic alteration, as well as at the veinward edge of some veins, implies that the ultimate stage of alteration and mineralization was reached during the growth of this assemblage: for the most part very near the late intrusive center of the district in a region characterized by the highest vein density and fracture permeability, the so-called horsetail zone. The sequence of mineralization types has been shown, by rock analysis (Brimhall, 1979), to include a protore stage (pyrite-chalcopyrite-magnetite) which with Main Stage circulation is progressively and systematically modified. A barren stage consisting of pyrite-quartz-sericite and no clay has been recognized as offering a possible source of copper for the Main Stage veins. This hypogene leaching has been followed in the western third of the district by pyrite-bornite assemblages and, ultimately, by chalcocite-covellite-sulfosalt assemblages (Brimhall, 1979). The progressive variations in mineral masses, when related to copper concentration, have provided a rigorous measure for reaction progress of Main Stage hydrothermal activity. The mass transfer "clocks" deduced in this fashion have made it possible to distinguish important substages of mineralization occurring within the Main Stage, with a resolution well above that of dating techniques. A major distinction is therefore offered between the geologic age date of an event and the value of the chemical reaction progress as determined by the mass transfer clocks based on lithologic analysis.

Thus we have an important separation of geologic time and chemical reaction progress, and can see that it is now possible to resolve individual chemical stages

TABLE 3. Stoichiometric Reaction Coefficients Used in Model Calculations for Reduced and Oxidized Forms of Sulfur Gas Contamination
(See Figures 9 and 10 for the position of joins A through E.)

Run no.	Effective valence	Stoichiometric reaction coefficients				
		$\nu_{Protore}$	$\nu_{H_2O_{(l)}}$	$\nu_{S_{2(g)}}$	$\nu_{O_{2(g)}}$	$\nu_{H_{2(g)}}$
				Join A: $O_{2(g)}$ or $H_{2(g)}$		
	[+4]	81.5		40.75	81.50	
27	[+3]	81.5	13.5833	40.75	61.25	
25	[+2]	81.5	27.1667	40.75	40.75	
26	[+1]	81.5	40.75	40.75	20.375	
	[0]	81.5	54.33	40.75		
28	[−1]	81.5	27.166	40.75		54.33
	[−2]	81.5		40.7500		81.5000
				Join B: $O_{2(g)}$ or $H_{2(g)}$		
	[+4]	81.5		20.375	40.75	
	[+3]	81.5	6.79167	20.375	30.625	
30	[+2]	81.5	13.5833	20.375	20.375	
29	[+1]	81.5	20.375	20.375	10.1875	
	[0]	81.5	27.1667	20.375		
	[−1]	81.5	13.5833	20.375		27.1667
	[−2]	81.5		20.375		40.75
				Join C: $O_{2(g)}$ or $H_{2(g)}$		
	[+4]	81.5		81.50	163.00	
	[+3]	81.5	27.167	81.50	122.5	
33	[+2]	81.5	54.333	81.50	81.5	
32	[+1]	81.5	81.5	81.50	40.75	
	[0]	81.5	108.666	81.50		
31	[−1]	81.5	54.333	81.50		108.666
	[−2]	81.5		81.50		163.00
				Join D: $O_{2(g)}$ or $H_{2(g)}$		
	[+4]	81.5		244.5	489.00	
	[+3]	81.5	81.5	244.51	367.5	
	[+2]	81.5	163.0	244.5	244.5	
35	[+1]	81.5	244.5	244.5	122.25	
	[0]	81.5	326.0	244.5		
34	[−1]	81.5	163.0	244.5		326.0
	[−2]	81.5		244.5		489.0
				Join E: $O_{2(g)}$ or $H_{2(g)}$		
	[+4]	81.5		570.5	1,141.00	
	[+3]	81.5	190.167	570.5	857.5	
	[+2]	81.5	380.33	570.5	570.5	
	[+1]	81.5	570.5	570.5	285.25	
	[0]	81.5	760.67	570.5		
36	[−1]	81.5	380.33	570.5		760.67
	[−2]	81.5		570.5		1,141.00

within the temporal Main Stage hydrothermal event, including the position of the advanced argillic assemblage. If this assemblage formed, as discussed previously in this paper, by sulfur gas interaction with protore and ground water, then a nearly complete geochemical cycle of vein formation may be imagined. Figure 12 presents such a cycle which couples the formation of the advanced argillic assemblage by neutral valence sulfur contamination (zone II, points c-i) with an isothermal, isobaric back-reaction of this advanced argillic fluid mixing with the protore (points i–q) as shown in a previous paper (Brimhall, 1980). Notice especially that the advanced argillic assemblage occurs at an intermediate value of fluid/rock ratio, during the formation of the horsetail structures. Reading from right to left, we interpret the

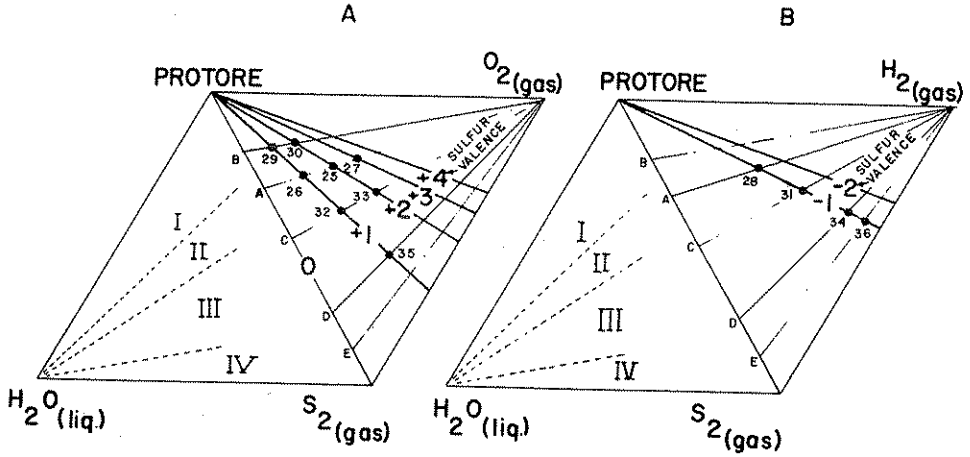

FIG. 10. Pair of diagrams showing the relationship of oxidized sulfur species (A) for valences of +1, +2, +3, and +4 relative to reduced species (B) for valences of −1 and −2. Computational gas reaction runs are as in Figure 9 and Table 3. In each triangle, i.e., protore-S_2-O_2 (A) and protore-S_2-H_2 (B), the oxidizing or reducing gas, O_2 or H_2, is rotated up over the H_2O-S_2-protore triangle and tetrahedrons are formed as shown in Figure 11.

sequence of vein-forming events essentially as a two-stage process. The initial event involves early Main Stage sulfur gas contamination of circulating ground water, ultimately yielding the advanced argillic assemblage by reactions of the zone II type. Protore feldspars are destroyed by direct sericite (muscovite) replacement with no intermediate development of clays (S type assemblage of Meyer et al., 1968), which for the most part is a very pyritic stage and quite often barren of copper mineralization, resulting in the development of a copper-charged vein-forming fluid, assuming of course a closed chemical system with respect to copper. When sulfur contamination essentially stops (point i, Fig. 12), the advanced argillic stage is reached at a minimum in pH and maxima in log f_{O_2} and log f_{S_2}. At this point also, the affinity of kaolinite is nearest zero (saturation). To the left of point i (Fig. 12), no $S_{2(g)}$ contamination occurs. Continued reaction of the fluid in equilibrium with the advanced argillic assemblage occurs farther out, producing points j through q, ultimately resulting in equilibrium with the wall-rock protore. Between i and the wall-rock equilibration point, the major vein-forming events occur. Notice the stair-stepped behavior in O_2 and S_2 fugacities as wall-rock mineral buffers progressively control fluid composition.

It is apparent in Figure 12 that the advanced argillic assemblage is a turning point in the chemical processes, as modeled. When this stage is reached, we have stopped $S_{2(g)}$ contamination and have allowed the system to relax chemically and to approach a state of equilibrium, i.e., once the acid vein-forming fluid is generated, simple reaction between it and its surroundings occur. The computed modal pattern is very close to that found in nature in many respects. For example, the shape of the kaolinite affinity curve implies near saturation only at the advanced argillic assemblage and after (to the left) during the Main State vein formation. This is consistent with an interpretation that the clay-free S type assemblage is slightly earlier than the hydrothermal events resulting in major vein formation of the Main Stage based on crosscutting vein patterns. It is worth noting, how-

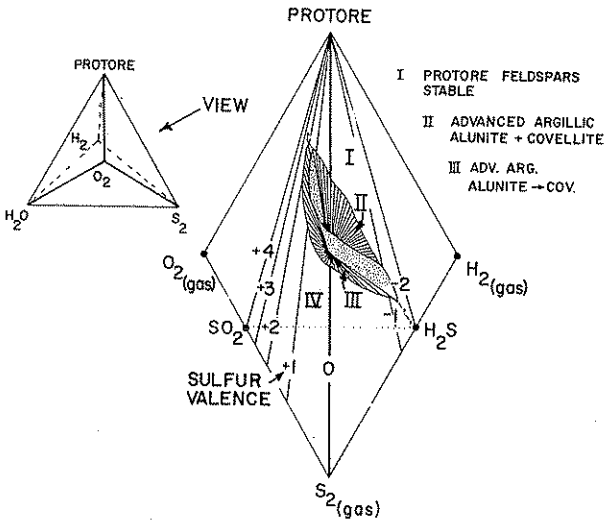

FIG. 11. Entire reaction schemes are represented (left) by a trigonal bipyramid with the upper O_2 (oxidized) apex directly above the lower H_2 (reduced) apex. The bipyramid as shown reveals the position of zones I to IV relative to O_2, SO_2, S_2, H_2S, and H_2 gases.

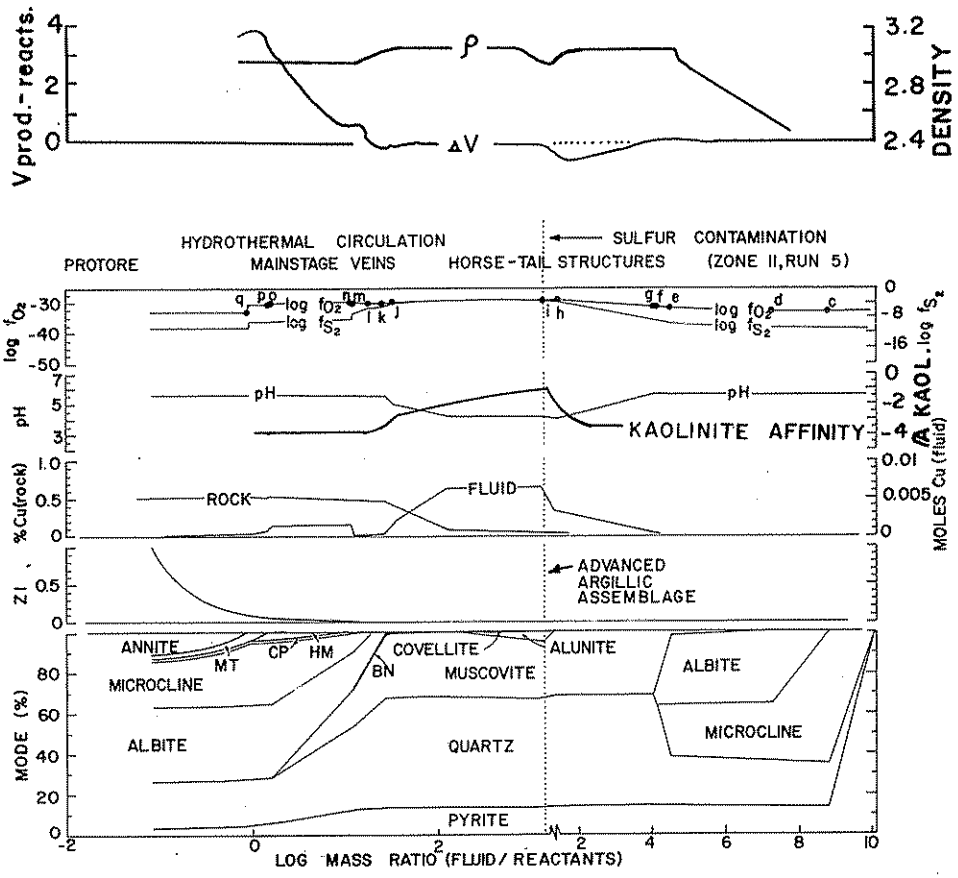

FIG. 12. Complete reaction cycle showing the generation of the advanced argillic assemblage at point (i) by sulfur gas contamination by zone II-type reactions (right half of the diagram), just after a minimum in the volume of products minus reactants. This negative ΔV may explain the high permeability attending the horsetail structures by chemical dissolution of wall rocks. To the left of point (i) fluids compatible with the advanced argillic assemblage, i.e., those with low pH, high f_{S_2} and f_{O_2}, continue to circulate and react with protore surroundings producing normal vein assemblages, ultimately reaching equilibrium with the protore (far left) as ΔV attains highest positive values. This may terminate fluid circulation by permeability reduction. Notice destruction of protore feldspars at intermediate values of the reaction progress. Note also the stabilization of a barren early pyrite-quartz-muscovite assemblage during the sulfur contamination event just preceding the advanced argillic assemblage.

ever, that this intermediate-age assemblage may have formed at temperatures somewhat above 300°C, and the lack of argillic alteration may be a temperature effect (J. J. Hemley, pers. commun.). Furthermore, the plot shown in Figure 12 of ΔV (products-solid reactants) has a local minimum slightly before the advanced argillic assemblage; this offers a potential explanation for enhanced rock permeability and extensive vein growth of the horsetail structures.

Interpretation of the Overall Reaction Path

It is possible to show quite effectively the main features of the computed reaction path in a coordinate system as shown in Figure 13 (Brimhall, 1980), using log $(a_{Fe^{+2}}/a^2_{Cu^+})$ vs. log $f_{H_2S_{(g)}}$. All sulfides and oxides occurring in the system are represented with phase boundaries given in Brimhall (1980). Using these coordinates (Fig. 14) the entire combined reaction path ($S_{2(g)}$ contamination plus back reaction) is represented by points a to q. The protore is shown as a solid hexagon (point a), the sulfur contamination path is a to i, the advanced argillic assemblage is at point i, and the major vein formation (back reaction) is along i to q. Contoured in Figure 14 is the log $f_{O_{2(g)}}$ shown as a surface with one mineral above and the subjacent mineral below (shown in parentheses) (Brimhall, 1980). Points on the reaction path which are above the f_{O_2} surface given, i.e., up into the field of pyrite alone, are shown with a plus sign (points e through k). Points falling right on the surface (separating the stability fields of two or more minerals) are shown as a solid dot (points k through q,

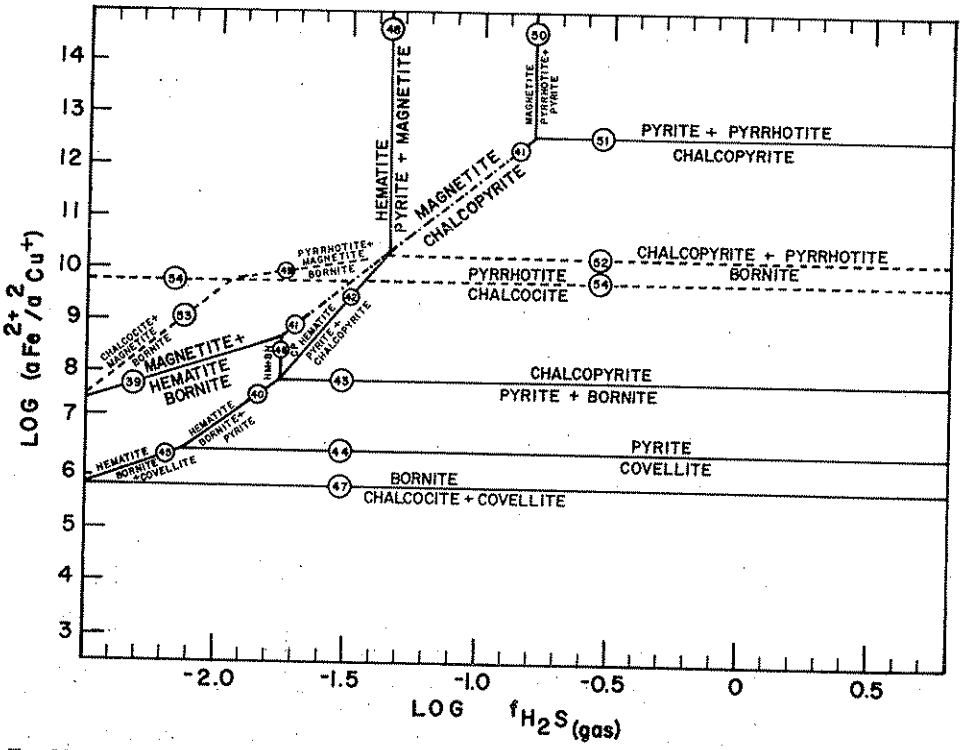

FIG. 13 Activity-fugacity diagram with major sulfide-oxide phase boundaries pertinent to the generation of acid-oxidizing fluids. Protore buffers fix both parameters, i.e., log $a_{(Fe^{+2}/a_{Cu^+}^2)}$ and log $f_{H_2S(g)}$ along the magnetite-chalcopyrite boundary. The pyrite-covellite phase boundary, typical of the advanced argillic assemblage, occurs at much lower iron to copper activity ratios than protore buffers.

which represent pyrite + bornite, pyrite + chalcopyrite, pyrite + chalcopyrite + hematite, and finally at the protore, pyrite + chalcopyrite + magnetite).

We see that the reaction path shown is a closed loop composed of two distinct segments; one originating at the protore and extending toward the advanced argillic assemblage and another extending back to the protore from the advanced argillic assemblage. The first path, i.e., the sulfidation path, is entirely above the phase boundary of pyrite with any other sulfide or oxide, implying very high oxygen fugacities within the pyrite field. The return leg of the path is exactly on the phase boundary of pyrite with other sulfides and oxides over most of its length. The position, relative to this oxygen fugacity surface, determines the stability of copper-bearing sulfides, and therefore, the nature of copper metasomatism. When the path is above the surface, in the pyrite field, copper is mobile in the aqueous phase. When the path is on the surface, copper is fixed as sulfides. Since pyrite is stable through the entire reaction loop, the path apparently never plunges down below the $f_{O_{2(g)}}$ surface into the field of a single sulfide or oxide besides pyrite.

It is worth noting that two segments of the reaction loop shown in Figure 14 may be characterized not only by their relative oxygen fugacity but also by their relative iron to copper activity ratio. The return path from the advanced argillic assemblage occurs at a log $(a_{Fe^{+2}}/a_{Cu^+}^2)$ much lower than the sulfur contamination path.

The relation of the two reaction path segments to the protore buffer mineral assemblage is shown in Figure 15 in which the stability field of annite component in protore biotite is shown contoured on log f_{O_2} (Brimhall, 1980) using the same representation as in Figure 14, i.e., with subjacent minerals given in parentheses (annite inside the volume overlain or surrounded by K-feldspar in addition to oxides and sulfides). The reaction loop originates on the annite surface with the coexistence of annite and K-feldspar. Upon sulfur metasomatism, the path abruptly departs from the annite volume and climbs to progressively higher oxygen fugacities until the advanced argillic assemblage is reached. If sulfur contamination stops at this point, back reaction occurs along the mineralization segment of the reaction path, at lower log $(a_{Fe^{+2}}/a_{Cu^+}^2)$ values than the oxidation-sulfidation

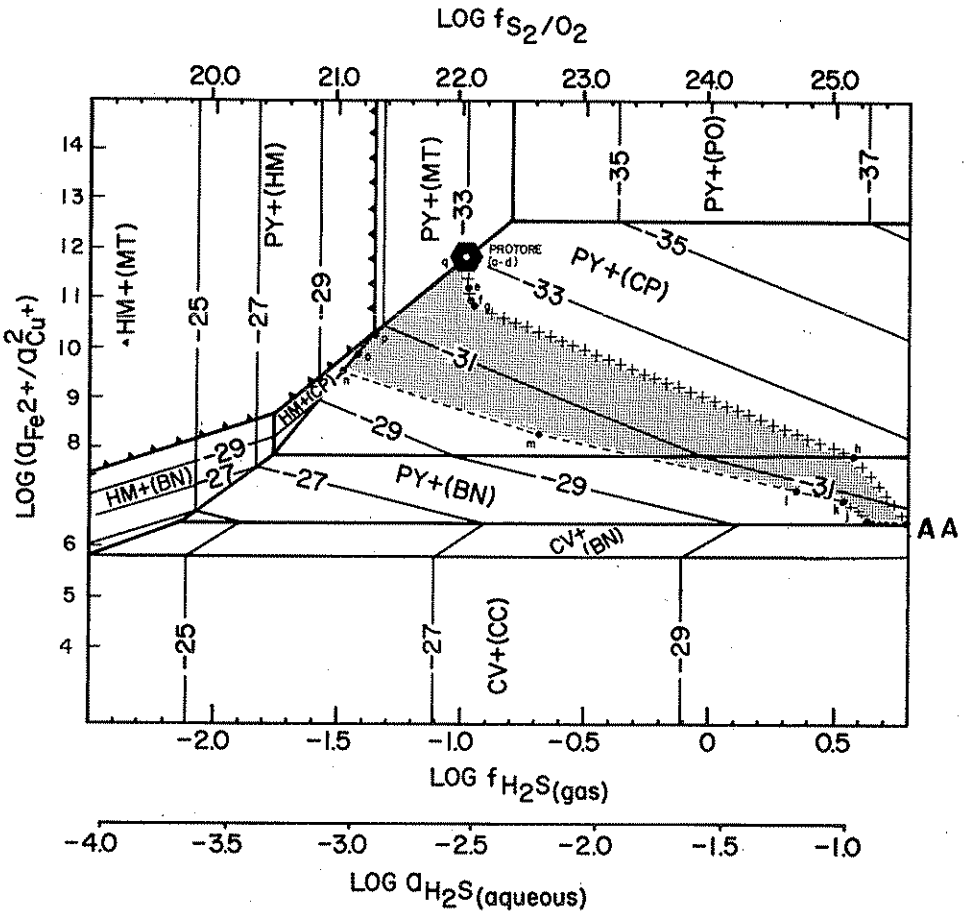

FIG. 14. Activity-fugacity diagram contoured on log $f_{O_{2(g)}}$ with phase boundaries as a pair of minerals, one above the f_{O_2} surfaces and one below (shown in parentheses), e.g., py + (cp) is pyrite at a higher f_{O_2} than chalcopyrite. Protore occurs at a log $f_{O_2} = -33$ at a temperature of 300°C and pressure of 500 bars. Points of interest are shown by letter along the reaction path given in Figure 12 (complete reaction cycle for advanced argillic assemblage). Points above oxidation boundaries are shown with a plus sign (+). Points on phases boundaries are shown with a dot signifying two coexisting minerals at a fixed log f_{O_2}. Barren quartz, pyrite, muscovite assemblage is the first to form. It occurs between point (e) and the advanced argillic assemblage (AA), which forms along the pyrite-covellite phase boundary (Fig. 13), at a log $f_{O_2} = -31$ much higher than the protore (log $f_{O_2} = -33$). Back reactions producing vein assemblages of the Main Stage form along the lower part of the stippled region, between the protore and point (i) after the advanced argillic assemblage (AA) has formed along the upper part of the stippled region. A complete reaction loop is shown.

path. Ultimately the annite volume is again reached at equilibrium with respect to the protore as attained.

Summary and Conclusions

Perhaps the most important aspect of the analysis presented in this study is the pivotal role of the advanced argillic assemblage in the geochemical evolution of the ore deposits at Butte which show attributes typical of several distinct types of ore-forming environments. The early or pre-Main Stage Cu-Mo mineralization and alteration sequences are clearly indicative of a fairly deep porphyry copper-type deposit. The Main Stage vein systems, however, reveal a late-stage hydrothermal event of enormous magnitude which exceeds the intensity and physical scale of the late hydrothermal collapse of meteoric fluids in more typical single-stage porphyry copper deposits in the southwestern United States. In these cases an "ore shell" is produced at the interface of the phyllic and potassic alteration zones.

It is significant that the advanced argillic assemblage occurs as an integral part of the Main Stage fluid evolution, both near normal veins as well as in the high density horsetail zones. Assuming that our

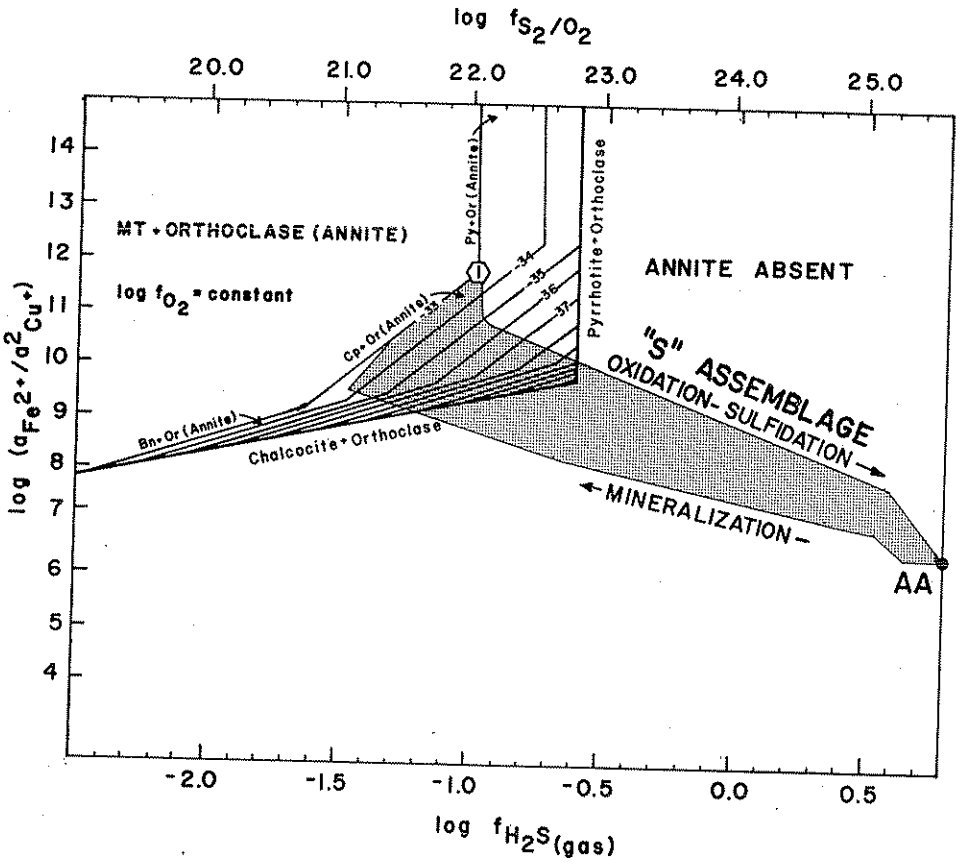

FIG. 15. Reaction loop (shown in Figure 14) in relation to the biotite (annite component) of the protore (Brimhall, 1980). Annite stability field is bounded in terms of log f_{O_2} contours, i.e., magnetite + orthoclase above, pyrhotite + orthoclase at high f_{H_2S}, and chalcocite + orthoclase at low Fe^{+2}/Cu^+ activity ratios. K-silicate protore (hexagon symbol) occurs right on the annite surface coexisting with magnetite + chalcopyrite + orthoclase + pyrite (Brimhall, 1980). The reaction loop extends out from this point: first along the upper leg of the loop through the barren S-type assemblage to the advanced argillic assemblage (AA) with pyrite and covellite, and subsequently along the lower leg of the loop producing normal Main Stage vein mineralization. Along both legs of the reaction loop, biotite of the protore must be destroyed before either excursion toward higher $f_{H_2S(g)}$ values can proceed. The upper barren leg of the reaction loop is essentially leaching copper from the wall-rock protore from chalcopyrite. Ultimately this same copper is fixed again in the form of high grade veins along the lower loop accompanied by a lower Fe^{+2}/Cu^+ activity ratio.

model is correct that the introduction of sulfur initiates the late-stage magmatic hydrothermal modification of the protore, then the role of the advanced argillic assemblage becomes somewhat clearer than was previously understood. Although the processes causing advanced alteration result in intense sericitization and silicification, it is evident from our thermodynamic calculations that permeability enhancement may be the critical mechanism by which fluids of dual origin, i.e., meteoric water and magmatic sulfur gases, are initially formed in a near-surface environment but then follow the thermally decaying heat source downward and encroach on hypogene environments. It is possible that these deeply circulating acid and oxidizing fluids in and around the horsetail structures and late intrusions shown in Figure 16 caused the remobilization of major amounts of copper from the deep low-grade K-silicate protore. A barren assemblage of quartz-sericite-pyrite of intermediate age between the protore and Main Stage veins is consistent with an early leaching of copper from the wall rock as the hydrothermal fluid was becoming richer in sulfur (arsenic, tellurium, bismuth, gold, silver, etc.) and acid constituents, i.e., evolving into compatibility with the advanced argillic alteration assemblage near the heat source. Upon attainment of the permeability maximum, it is likely that normal Main Stage vein formation began. As the

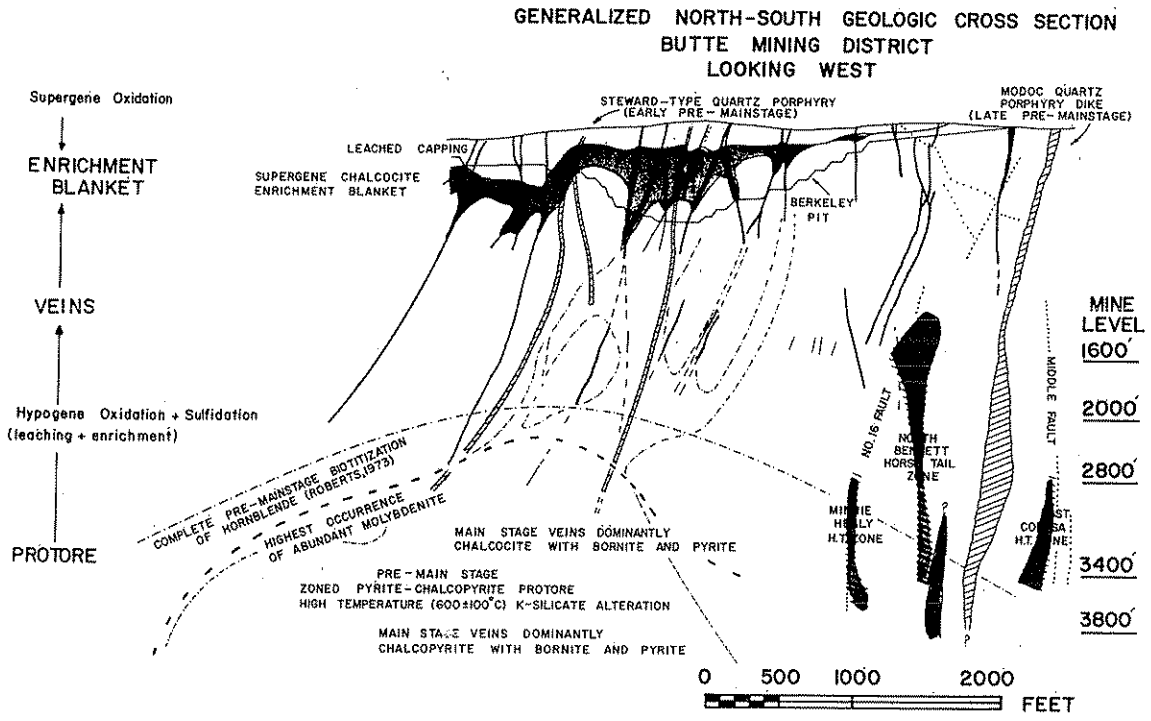

FIG. 16. Generalized north-south vertical cross section through the Butte district west of the Continental fault (Brimhall, 1979, 1980), showing distribution of protore, Main Stage veins, horsetail zones, and late intrusives relative to weathering surface and supergene enrichment blanket exposed in the Berkely pit (MacClave, 1973). Zone of early protore-related, biotization of hornblende is shown (Roberts, 1973) relating to the copper-molybdenum dome (Meyer et al., 1968). Essential features to be noted are the distribution of pre-Main Stage protore shown by upper occurrence of obvious molybdenite (Meyer et al., 1968) and the Central zone horsetail structures between fault 16 and the middle faults. Most likely intrusives, or at least their uppermost dike systems responsible for local Main Stage fluid circulation, are the Modoc quartz porphyry dikes, which are displaced from the 5-m.y. older protore dome structure containing the early fracture-controlled disseminated sulfide mineralization formed at much higher temperatures than the Main Stage veins (Brimhall, 1979, 1980). Major remobilization of copper apparently was in an upward direction from the protore, at least in the exposed part of the district, resulting in a major enlargement in the vertical and horizontal dimensions of the original zone of mineralization.

large veins formed, the source of energy for the fluid convection probably was continuously dissipating and encroachment of the near-surface advanced argillic environment occurred in a downward direction following the decaying heat source.

The ultimate effect of the apparent superposition of a young magmatic hydrothermal system upon an older, thermally inactive system (protore) was an enlargement of the vertical and lateral dimension of the deposit. In addition, the Main Stage vein growth may be considered as a coupled leaching and enrichment phenomena, producing higher grade ore in continuous mineable structures which extend upward to the present surface. Supergene enrichment of these veins (MacClave, 1973) has produced quite recently a chalcocite enrichment blanket of considerable size. Viewed in this way the evolution of the district into its present form may help to illuminate other deposits which seem to show, in present exposures, only one phase comparable with the multistage ore deposit at Butte, Montana.

In this paper, using a necessarily oversimplified approach, we do not claim to have solved all the major problems in the generation of highly acid crustal fluids. We have, nevertheless, established a definite genetic relationship between the advanced argillic alteration assemblage and a number of important physical and chemical parameters which undergo extreme behavior at this critical stage of geochemical evolution. Included in the unusual effects are a minimum in solution pH, maxima in fugacities of O_2 and S_2, and chemical enhancement of permeability or porosity as indicated by a negative volume of reaction. We suggest, therefore, that the advanced argillic assemblage represents a critical transition state or threshold, which if attained in a given hydrothermal system creates a very special environment of greatly enhanced fluid flow, alteration, and ore de-

position, including chemical mechanisms for self-sealing and ore preservation.

Acknowledgments

Discussions with Ian Carmichael and computer time made available by him on the Lawrence Livermore Berkeley Laboratory CDC 7600 computer contributed significantly to this study. The illuminating experimental efforts of J. J. Hemley on the stability of alunite inspired this effort. The research described in this paper has been generously supported by NSF grants EAR 79-11342 and EAR 81-15907.

October 16, 1981; May 26, 1982

REFERENCES

Brimhall, G. H, Jr., 1977, Early fracture-controlled disseminated mineralization at Butte, Montana: ECON. GEOL., v. 72, p. 37–59.

—— 1979, Lithologic determination of mass transfer mechanisms of multiple-stage porphyry copper mineralization at Butte, Montana; vein formation by hypogene leaching and enrichment of potassium-silicate protore: ECON. GEOL., v. 74, p. 556–589.

—— 1980, Deep hypogene oxidation of porphyry copper potassium-silicate protore at Butte, Montana: A theoretical evaluation of the copper remobilization hypothesis: ECON. GEOL., v. 75, p. 384–409.

Burnham, C. Wayne, 1979, Magmas and hydrothermal fluids, *in* Barnes, H. L., ed., Geochemistry of hydrothermal ore deposits: New York, John Wiley and Sons, p. 71–136.

Burnham, C. Wayne, and Ohmoto, H., 1980, Late stage processes of felsic magmatism: Soc. Mining Geologists Japan, Spec. Issue 8, p. 1–12.

Chappell, B. W., and White, A. J. R., 1974, Two contrasting granite types: Pacific Geology, v. 8, p. 173–174.

Helgeson, H. C., 1968, Evaluation of irreversible reactions in geochemical processes involving minerals and aqueous solutions—I. Thermodynamic relations: Geochim. et Cosmochim. Acta, v. 32, p. 853–877.

—— 1971, Kinetics of mass transfer among silicates and aqueous solutions: Geochim. et Cosmochim. Acta, v. 35, p. 421–469.

Helgeson, H. C., Delany, J. M., Nesbitt, H. W., and Bird, D. K., 1978, Summary and critique of the thermodynamic properties of rock-forming minerals: Am. Jour. Sci., v. 278-A, p. 1–229.

Hemley, J. J., and Jones, W. R., 1964, Chemical aspects of hydrothermal alteration with emphasis on hydrogen metasomatism: ECON. GEOL., v. 59, p. 538–569.

Hemley, J. J., Hostetler, P. B., Gude, A. J., and Mountjoy, W. T., 1969, Some stability relations of alunite: ECON. GEOL., v. 64, p. 599–612.

Hemley, J. J., Montoya, J. W., Marinenko, J. W., and Luce, R. W., 1980, Equilibria in the system Al_2O_3-SiO^2-H_2O and some general implications for alteration/mineralization processes: ECON. GEOL., v. 75, p. 210–228.

Hollister, V. F., 1978, Geology of the porphyry copper deposits of the western hemisphere: New York, Am. Inst. Mining Metall. Petroleum Engineers, p. 29, 137.

MacClave, M. A., 1973, Control and distribution of supergene enrichment in the Berkeley pit, Butte district, Montana, *in* Miller, R. N., ed., Guidebook for the Butte field Meeting, Society Economic Geologist: Butte, Montana, The Anaconda Company, p. K1–K4.

Meyer, C., and Hemley, J. J., 1967, Wall rock alteration, *in* Barnes, H. L., ed., Geochemistry of hydrothermal ore deposits: New York, Holt, Rinehart and Winston, p. 166–235.

Meyer, C., Shea, E. P., Goddard, C. C., Jr., and staff, 1968, Ore deposits at Butte, Montana, *in* Ridge, J. D., ed., Ore deposits of the United States, 1933–1967 (Graton-Sales vol.): New York, Am. Inst. Mining Metall. Petroleum Engineers, v. 2, p. 1363–1416.

Petersen, U., 1980, Metallogenesis in South Africa: Progress and problems; Episodes, v. 1979, no. 4, p. 3–11.

Roberts, S. A., 1973, Pervasive early alteration in the Butte district, Montana, *in* Miller, R. N., ed., Guidebook for the Butte field meeting, Society Economic Geologists: Butte, Montana, The Anaconda Company, p. HH-1–HH-8.

Sheppard, S. M. F., and Taylor, H. P., Jr., 1974, Hydrogen and oxygen isotope evidence for the origins of water in the Boulder batholith and the Butte ore deposits, Montana: ECON. GEOL., v. 69, p. 926–946.

Taylor, H. P., Jr., 1974, The application of oxygen and hydrogen isotope studies to problems of hydrothermal alteration and ore deposition: ECON. GEOL., v. 69, p. 843–883.

Wallace, A. B., 1979, Possible signatures of buried porphyry copper deposits in middle to late Tertiary rocks of western Nevada: Nevada Bur. Mines Rept. 33, I.A.G.O.D. papers on Mineral Deposits of Western North America, p. 69–76.

—— 1980, Geochemistry of polymetallic veins and associated wall rock alteration, Pyramid district, Washoe County, Nevada: Mining Eng., March, p. 314–320.

White, D. E., 1957, Thermal waters of volcanic origin: Geol. Soc. America Bull., v. 68, p. 1637–1657.

Wolery, T. J., 1979, Calculation of chemical equilibrium between aqueous solution and minerals: The EQ3/6 soft-wares package: Univ. California Lawrence Livermore Lab. Bull. 52658, 31 p.